

# Invariance of Single-File Water Mobility in Gramicidin-like Peptidic Pores as Function of Pore Length

Guillem Portella,\* Peter Pohl,<sup>†</sup> and Bert L. de Groot\*

\*Computational Biomolecular Dynamics Group, Max Planck Institute for Biophysical Chemistry, Göttingen, Germany; and <sup>†</sup>Institute for Biophysics, University of Linz, Linz, Austria

**ABSTRACT** We investigated the structural and energetic determinants underlying water permeation through peptidic nanopores, motivated by recent experimental findings that indicate that water mobility in single-file water channels displays nonlinear length dependence. To address the molecular mechanism determining the observed length dependence, we studied water permeability in a series of designed gramicidin-like channels of different length using atomistic molecular dynamics simulations. We found that within the studied range of length the osmotic water permeability is independent of pore length. This result is at variance with textbook models, where the relationship is assumed to be linear. Energetic analysis shows that loss of solvation rather than specific water binding sites in the pore form the main energetic barrier for water permeation, consistent with our dynamics results. For this situation, we propose a modified expression for osmotic permeability that fully takes into account water motion collectivity and does not depend on the pore length. Different schematic barrier profiles are discussed that explain both experimental and computational interpretations, and we propose a set of experiments aimed at validation of the presented results. Implications of the results for the design of peptidic channels with desired permeation characteristics are discussed.

## INTRODUCTION

Pores play a fundamental role in nature as well as in nanotechnological applications. Life could not exist without boundaries separating the inner part of the cell from the surroundings. However, cell membranes must be permeable to interact with the environment. Endo- and exocytosis are mechanisms to introduce large amounts of matter into the cell by membrane fusion. However, in some cases, fine-tuning of the transport process is needed to maintain microscopic balance or imbalance. Proton gradients, for example, are indispensable for bioenergetics. Also, specific release and uptake of ions by cells are crucial for keeping the desired electrochemical properties of solutions, with intricate consequences for metabolism. This precise functionality is achieved by membrane-spanning proteic and peptidic pores. Depending on their function, pores vary in dimension, specificity, and turnover rates. To achieve selectivity when it is required, nature has developed a variety of mechanisms (1) to filter desired molecules (or even atoms) without compromising efficiency. In some cases, selectivity is accomplished by suitable pore size in conjunction with electrostatic barriers (2–4).

The small antibiotic peptide gramicidin A, for example, is known to selectively permeate monovalent cations along with water. This selectivity makes gramicidin A channel very interesting as a sensitive detector and has already been used for the detection of protein-ligand interactions (5). The small diameter of this pore (4 Å) accounts for its selectivity, because even small molecules like urea cannot fit in its lumen.

Confinement of water by channel geometry to a one-dimensional file of molecules interacting with the pore alters its physical characteristics, e.g., liquid-vapor oscillations (6,7). Furthermore, since water ordering inside single-file channels modulates proton conductance via a proton-wire hydrogen-bonding network (8), possible applications of narrow, single-file water pores include switchable nanoscale conductors. The theoretical machinery required for understanding water permeation needs to explicitly take into account the microscopic nature of transport.

Recent experimental results (9) indicated that single-file water channels show an exponential dependence of water mobility on the file length: reduction of pore occupancy by one water molecule drastically enhanced water mobility. Using gramicidin derivatives of different pore length, an exponential increase on water permeability as the channel shortens was reported. This dependence is at variance with the classic result from Finkelstein (10,11), which assumes a linear relationship.

On the basis of these experimental findings and the long accepted linear prediction, we decided to investigate the microscopic details of the connection between water mobility and pore length. Taking advantage of computer modeling, we carefully designed a series of peptidic pores of different length with directly comparable structural features embedded in an artificial membrane of controlled width, and characterized them using extensive atomistic molecular dynamics simulations. In doing so, we restricted the structural variations among compared channels solely to the length, making sure that secondary effects, like potential distortions due to sequence difference, membrane thickness, and capping groups, did not bias the results.

Submitted December 12, 2006, and accepted for publication February 12, 2007.

Address reprint requests to B. L. de Groot, Tel.: 49-551-201-2308; email: bgroot@gwdg.de.

© 2007 by the Biophysical Society

0006-3495/07/06/3930/08 \$2.00

doi: 10.1529/biophysj.106.102921

The present study is discussed in the light of osmotic permeability ( $p_f$ ) and diffusion permeabilities ( $p_d$ ) as a means of quantifying water mobility inside single-file pores (10). The value  $p_f$  is related to the intrinsic water flux inside the pore (12,13), while  $p_d$  represents a net water transport between the compartments linked by the pore. Water mobility is therefore clearly related to the osmotic permeability coefficient, and the latter in return is related with  $p_d$  via the occupation number (10). To be able to elucidate structural determinants, we evaluated water free-energy profiles and interaction profiles along the water pathway.

The length dependence of instantaneous water flux in the length range investigated (1.4–2.5 nm) is discussed, and we propose different underlying energetic schemes consistent with the different observed behaviors, both experimental and computational.

## THEORY AND METHODS

### Design and setup

For the design of model pores to test the relationship between water flux and length, it is crucial to separate the effects arising from other sources, such as linking groups with different conformations, channel symmetry, width of the lipid bilayer, etc. We regularized a set of D,L polyaniline peptides with a typical  $\beta$ -helix gramicidin A folding motif, embedded in a membrane slab of adjustable thickness to avoid side effects due to nonmatching lipid membranes.

Seven single-file water pores have been prepared using one monomer of gramicidin A in head-to-head helical dimer conformation as a template (Fig. 1). The template was constructed by averaging the available NMR structures (PDB codes 1GRM, 1JNO, 1MAG, 1NRM, 1NRU (14–16)) and setting all hydrogen-bond distance between helix planes to the mean value to remove irregularities. All the residues were mutated to alanine to guarantee a set of directly comparable peptides, while keeping the capping groups formyl and ethanolamine at the N- and C-termini, respectively. Due to the alternating D,L amino-acid sequence, the side chains point outwards from the pore lumen and do not affect the hydrophilic environment inside the pore caused by the amino-acid backbone. The role of the side chains is to keep the structure stable and anchor the pore within the membrane (17–19). The

integrity of the folded structure was ensured by softly restraining the dynamics of the backbone and of the capping group atoms to their respective starting conformation using harmonic restraint forces of 500 kJ/mol/nm<sup>2</sup>.

The shortest unit, p-ala15, is then a mutated version of a gramicidin A monomer in helical dimer conformation. We generated longer pores by increasing the number of amino acids in the sequence of the previous template in steps of two. Up to p-ala21, residues were added by extending the template from the C-terminus. To obtain longer pores (p-ala23 to p-ala27), p-ala21 was additionally extended toward the N-terminus. After energy minimization with position restraints on the peptide main chain, the structures were inserted in a membrane. Using this procedure, propagation of inhomogeneities in building the three-dimensional arrangement is minimized, since all channels are directly based on the same template.

The disturbances of the pore caused by the membrane can be quite drastic, and affect pores of varying length to different extents (12,20,21). For a controlled environment, it is necessary to adjust the membrane according to the pore it accommodates. To do so, we devised an artificial membrane of octane molecules. This membrane offers the possibility to modulate its thickness via molecular-dynamics pressure coupling, adjusting itself to the height of the inserted pore. The simulation systems were set up as follows. First, a simulation box filled with water was generated around the peptide. Then, a slab of water molecules was removed to accommodate the membrane. Next, octane molecules were added to the empty compartment. A short (~150 ps) molecular dynamics equilibration was performed using pressure coupling and keeping the peptide fixed by means of strong position restraints (5000 kJ/mol/nm<sup>2</sup> harmonic force constant to all atoms), finally obtaining a constant density and desired width for the octane slab. To keep the membrane stable over the course of simulations, we performed all molecular dynamics production runs using constant volume.

Interactions between all atoms in octane and peptides were described by means of the OPLS all-atom force field (22,23) and water molecules were described by the TIP4P model (24). A set of control simulations was carried out using the simple-point-charge water model (25). All simulations were performed using the GROMACS simulation software (26,27). Electrostatic interactions were calculated with the particle-mesh Ewald method (28,29). Short-range repulsive and attractive dispersion interactions were simultaneously described by a Lennard-Jones potential, using a cutoff length of 1.0 nm. The SETTLE (30) algorithm was used to constrain bond lengths and angles of water molecules, and LINCS (31) was used for all other bonds and angles, allowing a time step of 2 fs. The temperature in the simulations was kept constant by weakly coupling the peptide, octane, and water molecules to an external heat bath at 300 K (32). When constant pressure simulations were required, a weak coupling to a pressure bath of 1 atm was used.

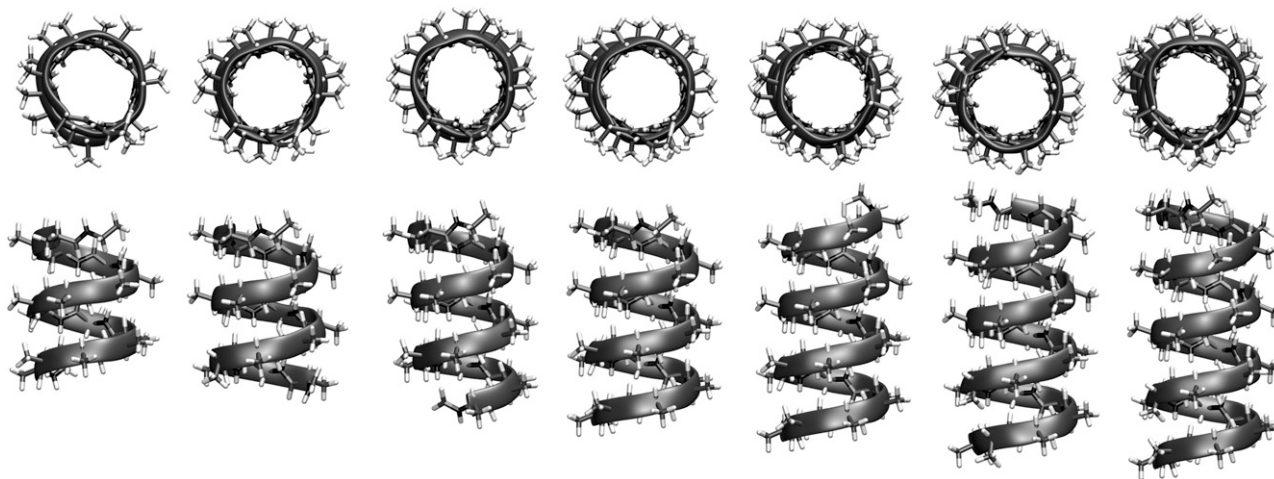


FIGURE 1 Top and side view of the seven modeled polyaniline pores, of increasing number of residues, used for the study.

All simulations were run for 100 ns. The simulations with TIP4P water model were repeated twice, using different starting velocities to enhance statistics. The total simulation time amounted to 2.1  $\mu$ s.

## Single-file water transport coefficients

To describe the mobility of water molecules inside single-file water pores we used the osmotic permeation coefficient ( $p_f$ ) and the diffusion permeation coefficient ( $p_d$ ).

The value  $p_f$  relates the total water flux ( $j_w$ ) through a channel to the osmotic gradient  $\Delta C_s$ , according to  $j_w = p_f \Delta C_s$ . Although we perform our molecular dynamics runs in absence of an osmotic gradient, it is possible to compute nonequilibrium water permeabilities like  $p_f$  from these equilibrium simulations (12,33). The average water column mobility is an intrinsic property of the pore, which can be rationalized in thermodynamic equilibrium as a one-dimensional unbiased random walk (33). In presence of an osmotic gradient, an imbalance of the water chemical potential will bias the water displacements according to the concentration gradient. In this situation a net flux of water molecules is established,  $j_w$ , proportional to the diffusion constant of the water column along a collective coordinate computed from the equilibrium simulations (33). If we assume that the water molecules in the single file exhibit perfectly correlated motions, rate theory can be applied on the collective coordinate defined by the water chain. In this case, one water molecule is effectively displaced from one compartment to the other when the column travels a water-water distance, corresponding to one  $p_f$ -event. It is possible to calculate the permeation coefficient in a perfectly correlated water column as  $p_f = \frac{1}{2} \Phi_0 \nu_w$ , where  $\Phi_0$  is the intrinsic flux and  $\nu_w$  the molar water volume (12,13). The intrinsic flux is here defined as the number of bidirectional collective jumps of the water column about a water-water distance (taken as 2.75 Å). The validity of this approximation is subject to the condition that the pore is always completely occupied. For water transport in pores featuring vacancies, other models (34,35) should be considered. We tested the above collective approach by comparing to the  $p_f$  obtained by counting events that corresponded to entry and exit of water molecules from opposite sides. Such motions, not necessarily correlated, contribute to the measured  $p_f$  in the presence of an osmotic gradient. We found quantitative agreement between the two measurements for  $p_f$  and chose the method of counting bidirectional collective jumps for calculating  $p_f$  in the rest of this work.

The textbook analytical expression

$$p_f = \frac{\pi r^2 D_w}{L}, \quad (1)$$

as collected from Finkelstein and Rosenberg (11), shows a linear relationship between osmotic permeability coefficient and pore length  $L$  via  $D_w$ , the average diffusivity a water molecule would have if it would be alone in the pore. The value  $r$  is the radius of the pore. The value  $D_w$  is assumed to be independent of  $L$ . The arguments used for the derivations are grounded on the thermodynamic work driven by the osmotic pressure and the frictional force opposing the water transport. Since every molecule of the water column was assumed to experience the same additive frictional force, the velocity of the column was suggested to decrease linearly with  $L$ . It is important to note that the assumptions that lead to Eq. 1 implies that the pore is fully occupied with noninteracting water molecules, so that the collectivity of water motion is not taken into account. In this work, we will study the validity of this result.

The diffusion permeation coefficient,  $p_d$ , describes the equilibrium flux between two compartments of equal concentration. The relation is assumed to be  $j_d = p_d \Delta C_d$  (10), where  $j_d$  is the net diffusive flux, and  $\Delta C_d$  indicates a concentration gradient of labeled water molecules with identical interaction properties with the pore and the rest of the solvent. In this regime, a permeation event consists of the transport of a given water molecule from one side of the channel to the other. Similar to  $p_f$ , the diffusion permeation coefficient is computed as  $p_d = \frac{1}{2} \Phi_c \nu_w$  (13), where  $\Phi_c$  is the number of

bidirectional complete water translocations. Because complete permeation events are rare compared to water-water distance movements, we make use of the symmetry of the pore and count the number of water molecules crossing half of the pore to increase the statistical accuracy. Considering that it is four times more probable to travel half a distance than completing a full translocation passage, the number of complete permeations is one-fourth of the half-permeation events. We validated our approach by comparing the results obtained from both counting methods, with excellent agreement.

Within the single-file framework, the ratio between the two permeation coefficients in a fully occupied pore is assumed to be equal to  $N+1$  or  $N$  (11,13,36), where  $N$  is the number of single-file water molecules that fit into the channel. The exact relationship depends on the analytical model used to derive expressions for both permeation coefficients. Despite the different results proposed for the ratio between  $p_f$  and  $p_d$ , the expression linearly relates the number of permeation events that completely cross the channel to the number of positions a water molecule has to travel. The result naturally follows from casting the transport process as a continuous time random walk (37), implying memoryless jumps of the water column. For the rest of this work we used  $N+1$  as the proportionality factor, following the literature (13,37). The pore occupancy can be directly estimated from the simulations by averaging the number of water molecules within the pore over the simulation time. Cylindrical pore boundaries were used, defined by the radial cutoff imposed by the pore backbone and the averaged position of the first and last peptide's residue at every time step.

## Thermodynamic properties

Free energy profiles  $F(z)$  of water molecules moving along the pore axis (defined as the  $z$  axis) have been calculated using two different approaches. Since the production simulations were run at constant volume, we can directly access the Helmholtz free energy  $F(z)$  via the water number density  $\rho(z)$  as  $F(z) = -k_B T \ln \rho(z)$ , with  $k_B$  the Boltzmann's constant and  $T$  the temperature. The number density was evaluated in 0.1 Å bins over the simulation time. This approach yields the total contribution of the whole system to each single water molecule as it permeates the pore. To achieve a better understanding of the determinants affecting the transported molecules, we also calculated the potential energy surface along the pore axis by integration of the average forces acting on the single water molecule  $F(z) = \int_{z_1, \langle f_z(z_1) \rangle=0}^z \langle f_z(z') \rangle dz'$ , with  $z_1$  the reference position where the average force vanishes. Hence, we use the term of potential of mean force (PMF) for these profiles. This allows us to qualitatively assess contributions of the peptide and those imposed by the rest of water molecules by independently integrating the averaged forces involved in their interactions. Note that profiles of individual components do not necessarily reflect free energies, and can only be interpreted qualitatively.

It is worth stressing here that the picture obtained from such a free energy profile corresponds to the combined effects of water collectivity and interactions with the pore as well as the rest of the water. We validated the PMF procedure by comparing the profiles with the number-density result (see Fig. 5).

## Monte Carlo simulation on PMF

Water mobility in single-file pores is highly correlated. Therefore, water permeation can be treated as a collective motion of the single-file along the pore (Fig. 2). To characterize the relationship between the behavior and energetics of individual water molecules, we used Metropolis' Monte Carlo algorithm to move a chain of water molecules over a schematic potential energy surface. By considering the chain of water molecules as rigid, we introduced collectivity to the system. The step size was fixed, and adjusted to produce  $\sim 70\%$  accepted moves for barrier heights comparable to those extracted from our simulations. In this framework, a  $p_f$ -event is counted every time the water chain has crossed a water-water distance, and a  $p_d$ -event is computed when a water molecule has traveled the whole channel length.

Although no true rates can be computed by this approach, it provides useful relative information of the transport coefficients. If the step size is

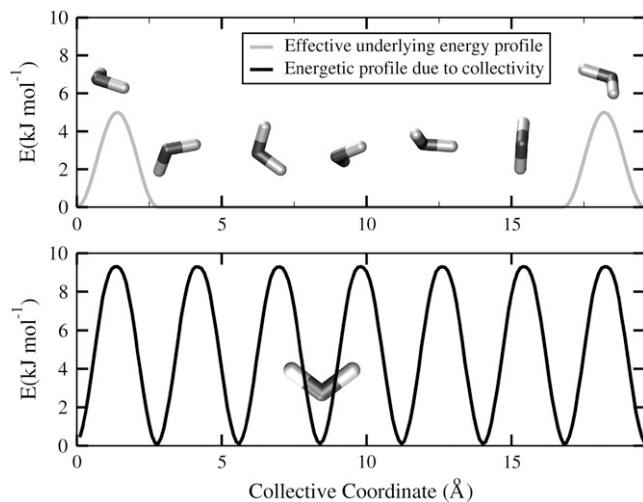


FIGURE 2 Effect of water collectivity on the underlying potential for motion along a single-file pore. The upper panel depicts a situation where two barriers are found at the entry/exit regions. The water molecules are sketched on top of the potential energy surface for illustration. Using the Monte Carlo method to sample the motion of a chain of water molecules, we can derive a free energy profile from the number density (*lower panel*). As a consequence of the imposed correlation between water positions, the emerging energetics seems to indicate the presence of local binding sites, whereas the true inner potential surface is actually flat.

kept constant for all channel lengths, a series of pores can be compared to obtain qualitative dynamic trends. This method is particularly useful to probe different underlying potentials by allowing us to screen various energetic scenarios for their compatibility with the MD results. It fully takes into account collectivity, and allows us to decompose obtained free energy profiles into contributions due to channel-water interaction and water-water correlation.

## RESULTS AND DISCUSSION

Fig. 3 shows the cumulative count of water-water displacements of the water column inside the pore as function of the simulation time. The slope of the curve is directly proportional to  $p_f$ . In all seven cases, the water flux displays a steady converged behavior and shows no clear dependence on pore length. In contrast, the cumulative number of complete water translocations from one side of the pore to the other (*inset*, Fig. 3) exhibits an overall decreasing slope with growing peptide length. The slope of the curve is in this case proportional to  $p_d$ .

Fig. 4 presents the osmotic permeability coefficient (Fig. 4 *a*) and the diffusion permeability coefficient (Fig. 4 *b*) as a function of the number of amino acids in the sequence, averaged over two independent sets of simulations. The osmotic permeability coefficient  $p_f$ , which is related to the intrinsic water mobility in the channel, is found to be independent on the length of the channel, within the simulation accuracy. Very low sensitivity of water flux and pore length was previously reported (38) for the osmotic water flow through carbon nanotubes.

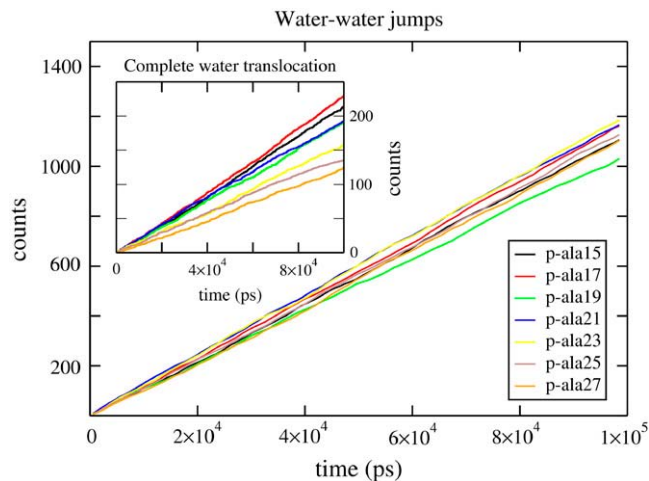


FIGURE 3 Cumulative water-water displacements (taken as 2.75 Å, *main frame*) and complete water translocation (after correcting for half-permeation counting, *inset*) for all seven pores studied, averaged over two independent simulations.

As expected, the diffusion permeability coefficient displays an inverse relationship with the length. In Fig. 4 *c*, we represent the water occupancy for each channel as a function of the number of residues. This can be directly estimated from the simulations (*red*) or computed via the relationship  $p_f/p_d = N + 1$  (*black*). Remarkably good agreement with both independent measurements is found. This is a strong indication that the assumptions of memoryless water jumps, completely filled pore, and water motion collectivity are indeed fulfilled.

The calculation of the free energy for permeating water (Fig. 5) reveals a main access barrier of  $\sim 3.6 \pm 0.2 k_B T$  for both pore entrances. Compared to this barrier, the energy required to move from one binding site to the next within the pore is small, in the order of  $k_B T$ . Similar behavior was also observed in carbon nanotubes (38). Results obtained via force integration or water density are nearly identical, as shown in the comparison panel for p-ala25 in Fig. 5.

Decomposition of free energy in water-water and water-protein interactions shows that both profiles are generally complementary, and loss of energy due to desolvation is partially counteracted by the attractive interaction with the peptide. Altogether, barriers due to solvent interaction are predominant. As the peptide grows in length, the fragment of the curve describing the inner part of the channel becomes flatter. Presumably the smoothing in the central channel region indicates that there is room for a noninteger number of water molecules in the channel. This would result in a deviation from the full correlation depicted in an idealized way in Fig. 2.

In a situation in which the barriers near the channel entry form the rate-limiting step for water permeation, the picture derived from decomposition of the interactions is consistent

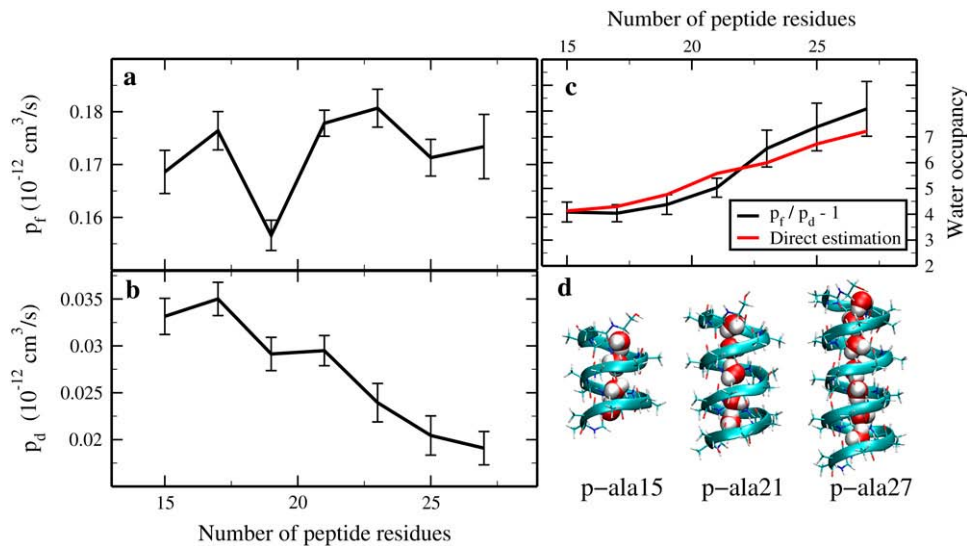


FIGURE 4 Averaged (a) osmotic permeability coefficient ( $p_f$ ) and (b) diffusive permeability coefficient ( $p_d$ ) from two independent simulations as function of the number of residues forming the channel. Panel c displays the relationship between residue number and water occupancy as computed via  $N = p_f/p_d - 1$  (black) and estimated from the simulation (red). Panel d illustrates water occupancy for p-ala15, p-ala21, and p-ala27.

with the dynamic result that the osmotic permeability coefficient is independent of the length of the single file.

To study the observed behavior in terms of the underlying free energy profile, we designed a number of schematic topologies for the potential of mean force. On these constructed profiles we characterized the behavior of the two transport coefficients,  $p_f$  and  $p_d$ , as a function of the single-file length via Monte Carlo sampling. In the first scenario, each water position was separated from the next one by a constant height barrier (Fig. 6, *two upper panels*). The barrier height represents the “binding” free energy of water in each mean occupation site, and no extra activation energy is required to access the pore. Increasing the number of water positions means adding new barriers. Depending on the

barrier height, two different regimes can be discerned. If the binding free energy is below thermal energy  $k_B T$  (Fig. 6, *first from the top*), the emerging picture corresponds to the textbook hypothesis of  $p_f \sim 1/N$  and therefore  $p_d \sim 1/N^2$ .

The result can be rationalized as follows: since the thermal energy of the system is above the binding free energy, the exponential dependence of the transition probability as function of the activation energy can be approximated linearly. Hence, the decay can be described as an inverse function of the activation energy, linearly dependent on the number of water molecules. Alternatively, if the activation energy for a water-water displacement is above the thermal energy (Fig. 6, *second from the top*), including more water molecules in the single file leads to an exponential dependence of both

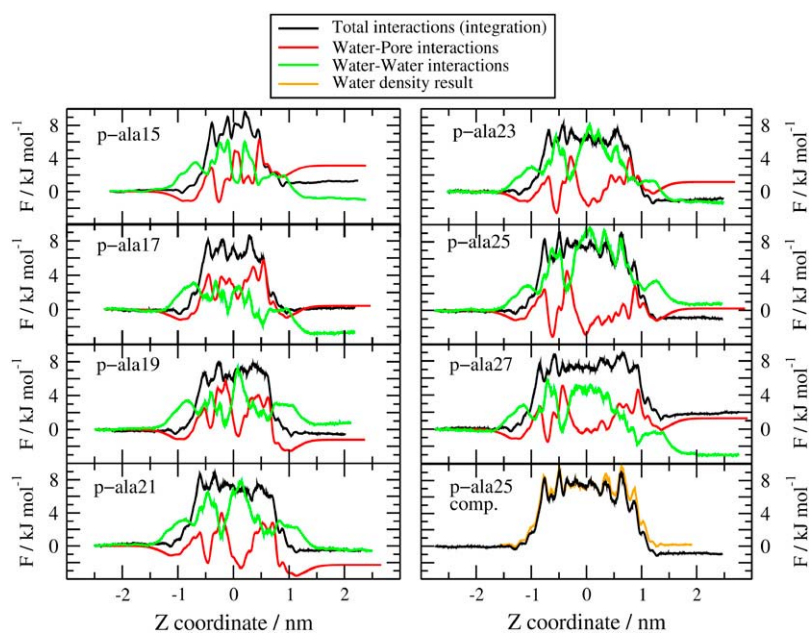


FIGURE 5 Free energy profiles and their decomposition for the series of peptidic pores as obtained from force integration (see text). Total interaction (black), water-pore interaction (red), and water-water interaction (green) are plotted against the main pore axis. The panel on the lower right shows a comparison of free energy profiles as computed via water number density (orange) with force integration (black) for p-ala25.

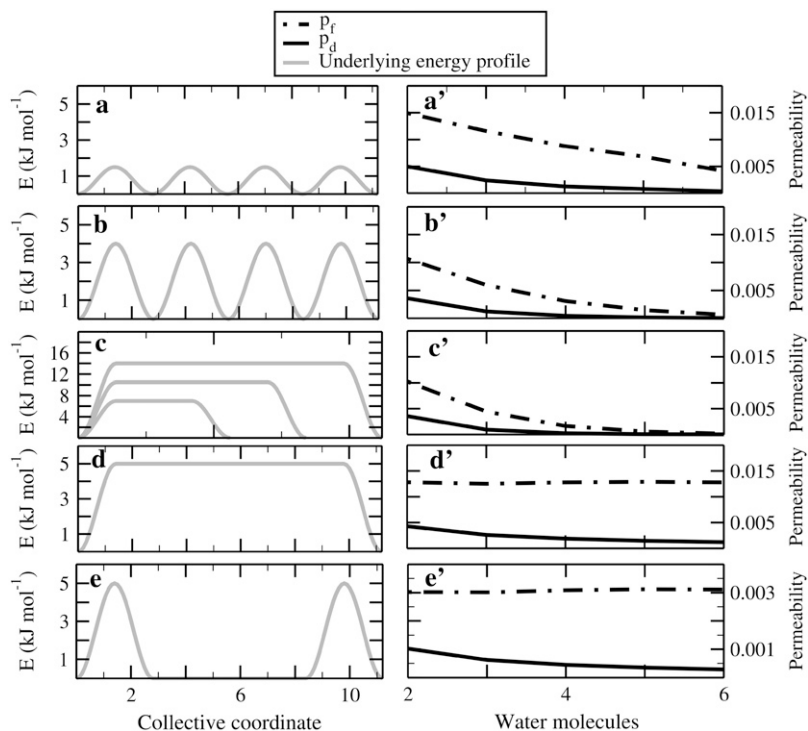


FIGURE 6 Different PMF schemes for a chain of water molecules permeating a single file pore (left, shaded) lead to a different length dependence (right), expressed in permeability coefficients  $p_f$  (dash-dotted) and  $p_d$  (solid). Only panels *d* and *e* are consistent with the simulation results, suggesting that no binding sites for individual water molecules are present within the pore, and that the main barrier is independent of pore length.

transport properties, similar to the experimental observations (9).

In the case of a single access barrier, such as in the last three profiles of Fig. 6, water mobility becomes dependent on the length of the single pore if the height of the barrier is variable. In such a situation, illustrated in Fig. 6 *c*, an exponential or linear dependence of water permeability is expected depending on the range of barrier heights, analogous to the situation in Fig. 6 *b*.

On the contrary, an access barrier with a fixed height displays water mobility independent of the single file length. The value  $p_d$  shows a characteristic inverse dependence, simply explained by a linear relationship between step size and coordinate length. As long as there is an access barrier, relative energies between inside/outside do not lead to formal differences in the expected dynamics of a highly correlated water file along a flat inner potential. This situation is consistent with the simulation results, and, in conjunction with the observed permeability behavior, suggests that the motion of the water column is governed by two or more access barriers or a central barrier of constant height. This hypothesis is further supported by the drastically altered water permeability found in gramicidin derivatives with mutated termini, as shown in desformyl gramicidin (12,39), or modified residues at the channel entry, such as lysin gramicidin (unpublished data).

In light of the obtained results, water permeability of gramicidin-like single-file peptidic water pores is length-independent. Hence, the simulation results suggest that, for the design of new channels, length is not a critical factor.

Corrections to Eq. 1 are mandatory to describe the observed behavior. A key assumption made in Eq. 1 is the independence of water molecules in the pore, i.e., interactions between water molecules are not taken into account. If we consider the collective nature of the water single-file column, every water-water displacement contributes one water molecule to the observed osmotic flux. Using the same procedure as in Finkelstein and Rosenberg (11) but identifying the water-water distance  $d_{ww}$  as the effective distance the water chain needs to travel to observe a flux of one water molecule, we arrive at

$$p_f = \frac{\pi r^2 D_c}{d_{ww}}, \quad (2)$$

where we use  $D_c$  as the effective diffusivity of chain of water molecules and  $r$  is the radius of the pore. Note that the obtained expression is indeed independent of the length of the pore or the number of water molecules.

The apparent discrepancy from the recent experimental findings (9) may be caused by simulation artifacts, like force-field inaccuracies. In a set of control simulations where we used the simple-point-charge water model instead of TIP4P, however, we saw qualitatively consistent results. Also, we cannot exclude the possibility that the osmotic pressure caused by the osmotic gradient induces conformational changes in the channel, an effect not captured by the present approach to obtain osmotic permeabilities from equilibrium simulations.

Alternatively, the great experimental variance of single-channel water permeabilities, which cover three orders of magnitude (40), is most probably not due to length changes.

Although the experimentally studied channels might have similar folding motifs, additional factors like unequal capping groups, differences in channel hydrophobicity, channel ability to form hydrogen bonds with permeating water molecules, membrane mismatch, or cross-link effects could lead to changes of the access barriers, and thus of permeability. Especially, interactions with the membrane are expected to play a major role in determining water permeability. Simulation studies have identified a strong influence on water permeability caused by interactions of lipid headgroups with the pore entrance (12,21). It would therefore be interesting to systematically study effects of the surrounding membrane or to modify membrane-channel interactions in the entry regions. A promising approach to investigate water permeation, recently applied in the design of ion channels (41), is the possibility to funnel the permeating molecules into the channel by means of ether coronas or similar derivatives. This way one could also partially diminish the effect of membrane mismatch and disturbances due to lipid headgroups.

Additional experiments will therefore be required to resolve this issue. Different assays on systems with varying bilayer width and constant gramicidin length would quantify the role of the external barriers on water permeability. Longer gramicidin-like channels should be experimentally measured for the validation of the different predictions based on the obtained results.

## CONCLUSIONS

To understand the main determinants of water permeation through single-file peptidic pores the influence of the channel length has been addressed. We designed a series of regularized D,L polyalanine peptides in a  $\beta$ -helix folding with increasing number of residues to isolate the effect of the channel length on the dynamics of water transport. The analysis of water mobility in terms of osmotic permeability ( $p_f$ ) reveals no dependence on the length of the pore. Accordingly, the diffusion permeability ( $p_d$ ) displays an inverse relationship with the length of the pore: at constant hopping rate, the longer the channel, the more time is needed for a complete translocation. This result is at variance with the classical view of a linear length dependence (10,11,42) and also with a recent experimental study that indicated an exponential length dependence (9). Inconsistencies of the proposed linear relationship can be corrected by identifying the displacement of the water column by a water-water distance as the effective transport step. The resulting expression becomes pore length-independent. To resolve the discrepancy with the exponential prediction, additional experiments are required.

The potential of mean force for a water moving along the channel main axis shows that the main barriers for water permeation are located at the channel entries. The main access barrier is  $\sim 3.6 k_B T$ , independent of the channel length. The water binding energies inside the pore are more than three times lower,  $\sim 1 k_B T$ . Decomposition of free energy in

water-water and water-peptide contributions identifies desolvation as the main origin of the access barrier.

Monte Carlo simulations on PMF allowed us to test different underlying energetic profiles and their consequences on the mobility depending on coordinate length. We identified three different types of behavior for  $p_f$  and  $p_d$  depending on the nature and position of the barriers. The simulation results are consistent with a situation where fixed height barriers are located in the channel entries: in this case, no correlation between channel length and water mobility is found.

Our results suggest that modifications, especially at the channel entry and exit, as well as controlled interactions of the channel with lipid headgroups, are critical determinants for water permeation. For the design of nanopores with desired permeation characteristics, this implies that channel hydrophobicity in the entry/exit region, and compatibility to the surrounding membrane, rather than channel length, are the major determinants underlying water permeability.

We thank Ira Tremmel for carefully reading the manuscript.

G.P. was supported via Deutsche Forschungsgemeinschaft grant No. GR-2079/2.

## REFERENCES

1. de Groot, B. L., and H. Grubmüller. 2001. Water permeation across biological membranes: mechanism and dynamics of Aquaporin-1 and GlpF. *Science*. 294:2353–2357.
2. Corry, B., and S. H. Chung. 2006. Mechanisms of valence selectivity in biological ion channels. *Cell. Mol. Life Sci.* 63:301–315.
3. Roux, B., and K. Schulten. 2004. Computational studies of membrane channels. *Structure*. 12:1343–1351.
4. Roux, B. 2005. Ion conduction and selectivity in  $K^+$  channels. *Annu. Rev. Biophys. Biomol. Struct.* 34:153–171.
5. Futaki, S., Y. J. Zhang, T. Kiwada, I. Nakase, T. Yagami, S. Oiki, and Y. Sugiura. 2004. Gramicidin-based channel systems for the detection of protein-ligand interaction. *Bioorg. Med. Chem.* 12:1343–1350.
6. Hummer, G., J. C. Rasaiah, and J. P. Noworyta. 2001. Water conduction through the hydrophobic channel of a carbon nanotube. *Nature*. 414:188–190.
7. Beckstein, O., and M. S. Sansom. 2003. Liquid-vapor oscillations of water in hydrophobic nanopores. *Proc. Natl. Acad. Sci. USA*. 100:7063–7068.
8. Pomès, R., and B. Roux. 1996. Structure and dynamics of a proton wire: a theoretical study of  $H^+$  translocation along the single-file water chain in the gramicidin A channel. *Biophys. J.* 71:19–39.
9. Saparov, S. M., J. R. Pfeifer, L. Al-Momani, G. Portella, B. L. deGroot, U. Koert, and P. Pohl. 2006. Mobility of a one-dimensional confined file of water molecules as a function of file length. *Phys. Rev. Lett.* 96:148101.
10. Finkelstein, A., and P. Rosenberg. 1979. Single-file transport: implications for ion and water movement through gramicidin A channels. *Membr. Transp. Processes*. 3:77–88.
11. Finkelstein, A. 1987. Water movement through lipid bilayers, pores, and plasma membranes. Wiley & Sons, New York.
12. de Groot, B. L., D. P. Tieleman, P. Pohl, and H. Grubmüller. 2002. Water permeation through gramicidin A: desformylation and the double helix; a molecular dynamics study. *Biophys. J.* 82:2934–2942.
13. Zhu, F. Q., E. Tajkhorshid, and K. Schulten. 2004. Theory and simulation of water permeation in aquaporin-1. *Biophys. J.* 86:50–57.

14. Lomize, A. L., V. I. Orekhov, and A. S. Arsen'ev. 1992. Refinement of the spatial structure of the gramicidin A ion channel. *Bioorg. Chim.* 18:182–200.
15. Townsley, L. E., W. A. Tucker, S. Sham, and J. F. Hinton. 2001. Structures of gramicidins A, B, and C incorporated into sodium dodecyl sulfate micelles. *Biochemistry.* 40:11676–11686.
16. Ketchum, R. R., B. Roux, and T. A. Cross. 1997. High-resolution polypeptide structure in a lamellar phase lipid environment from solid state NMR derived orientational constraints. *Structure.* 5:1655–1669.
17. dePlanque, M. R. R., J. A. W. Kruijtzter, R. M. J. Liskamp, D. Marsh, D. V. Greathouse, R. E. Koeppe, B. deKruijff, and J. A. Killian. 1999. Different membrane anchoring positions of tryptophan and lysine in synthetic transmembrane alpha-helical peptides. *J. Biol. Chem.* 274:20839–20846.
18. Jude, A. R., D. V. Greathouse, R. E. Koeppe, L. L. Providence, and O. S. Andersen. 1999. Modulation of gramicidin channel structure and function by the aliphatic “spacer” residues 10, 12, and 14 between the tryptophans. *Biochemistry.* 38:1030–1039.
19. Reithmeier, R. A. F. 1995. Characterization and modeling of membrane-proteins using sequence-analysis. *Curr. Opin. Struct. Biol.* 5:491–500.
20. Galbraith, T. P., and B. A. Wallace. 1998. Phospholipid chain length alters the equilibrium between pore and channel forms of gramicidin. *Faraday Discuss.* 111:159–164.
21. Chiu, S.-W., S. Subramaniam, and E. Jakobsson. 1999. Simulation study of the gramicidin/lipid bilayer system in excess water and lipid. II. Rates and mechanism of water transport. *Biophys. J.* 76:1939–1950.
22. Kaminski, G. A., R. A. Friesner, J. Tirado-Rives, and W. L. Jorgensen. 2001. Evaluation and reparameterization of the OPLS-AA force field for proteins via comparison with accurate quantum chemical calculations on peptides. *J. Phys. Chem. B.* 105:6474–6487.
23. Jorgensen, W. L., D. S. Maxwell, and J. Tirado-Rives. 1996. Development and testing of the OPLS all-atom force field on conformational energetics and properties of organic liquids. *J. Am. Chem. Soc.* 118:11225–11236.
24. Jorgensen, W. L., J. Chandrasekhar, J. D. Madura, R. W. Impey, and M. L. Klein. 1983. Comparison of simple potential functions for simulating liquid water. *J. Chem. Phys.* 79:926–935.
25. Berendsen, H. J. C., J. P. M. Postma, W. F. van Gunsteren, and J. Hermans. 1981. Interaction models for water in relation to protein hydration. In *Intermolecular Forces*. B. Pullman, editor. D. Reidel Publishing Company, Dordrecht, The Netherlands.
26. Lindahl, E., B. Hess, and D. Van der Spoel. 2001. GROMACS 3.0: a package for molecular simulation and trajectory analysis. *J. Mol. Model. (Online).* 7:306–317.
27. Van der Spoel, D., E. Lindahl, B. Hess, G. Groenhof, A. E. Mark, and H. J. C. Berendsen. 2005. GROMACS: fast, flexible and free. *J. Comput. Chem. (Online).* 26:1701–1718.
28. Darden, T., D. York, and L. Pedersen. 1993. Particle mesh Ewald: an  $N\text{-log}(N)$  method for Ewald sums in large systems. *J. Chem. Phys.* 98:10089–10092.
29. Essmann, U., L. Perera, M. L. Berkowitz, T. Darden, H. Lee, and L. G. Pedersen. 1995. A smooth particle mesh Ewald potential. *J. Chem. Phys.* 103:8577–8592.
30. Miyamoto, S., and P. A. Kollman. 1992. SETTLE: an analytical version of the SHAKE and RATTLE algorithms for rigid water models. *J. Comput. Chem.* 13:952–962.
31. Hess, B., H. Bekker, H. J. C. Berendsen, and J. G. E. M. Fraaije. 1997. LINCS: a linear constraint solver for molecular simulations. *J. Comput. Chem.* 18:1463–1472.
32. Berendsen, H. J. C., J. P. M. Postma, A. DiNola, and J. R. Haak. 1984. Molecular dynamics with coupling to an external bath. *J. Chem. Phys.* 81:3684–3690.
33. Zhu, F., E. Tajkhorshid, and K. Schulten. 2004. Collective diffusion model for water permeation through microscopic channels. *Phys. Rev. Lett.* 93:224501.
34. Chou, T. 1998. How fast do fluids squeeze through microscopic single-file pores? *Phys. Rev. Lett.* 80:85–88.
35. Chou, T. 1999. Kinetics and thermodynamics across single-file pores: solute permeability and rectified osmosis. *J. Chem. Phys.* 110:606–615.
36. Hernandez, J. A., and J. Fischbarg. 1992. Kinetic analysis of water transport through a single-file pore. *J. Gen. Physiol.* 99:645–662.
37. Berezhkovskii, A., and G. Hummer. 2002. Single-file transport of water molecules through a carbon nanotube. *Phys. Rev. Lett.* 89:064503.
38. Kalra, A., S. Garde, and G. Hummer. 2003. Osmotic water transport through carbon nanotube membranes. *Proc. Natl. Acad. Sci. USA.* 100:10175–10180.
39. Saparov, S. M., Y. N. Antonenko, R. E. Koeppe II, and P. Pohl. 2000. Desformylgramicidin: a model channel with an extremely high water permeability. *Biophys. J.* 79:2526–2534.
40. Pohl, P. 2004. Combined transport of water and ions through membrane channels. *Biol. Chem.* 385:921–926.
41. Pfeifer, J. R., P. Reiss, and U. Koert. 2006. Crown ether-gramicidin hybrid ion channels: dehydration-assisted ion selectivity. *Angew. Chem. Int. Ed.* 45:501–504.
42. Longuet-Higgins, H. C., and G. Austin. 1966. The kinetics of osmotic transport through pores of molecular dimensions. *Biophys. J.* 6:217–224.